Ecological Modelling 495 (2024) 110803

Contents lists available at ScienceDirect

Ecological Modelling

journal homepage: www.elsevier.com/locate/ecolmodel

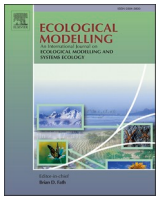

Individual-based modelling of adaptive physiological traits of cyanobacteria: Responses to light history

Mohammad Hassan Ranjbar [a,b,*], David P. Hamilton [a], Michael L. Pace [c], Amir Etemad-Shahidi [b,d], Cayelan C. Carey [e], Fernanda Helfer [b]

[a] Australian Rivers Institute, Griffith University, Queensland, Australia
[b] School of Engineering and Built Environment, Griffith University, Queensland, Australia
[c] Department of Environmental Sciences, University of Virginia, Charlottesville, Virginia, USA
[d] School of Engineering, Edith Cowan University, Western Australia, Australia
[e] Department of Biological Sciences, Virginia Tech, Blacksburg, Virginia, USA

ARTICLE INFO

Keywords:
Agent-based modelling
Dolichospermum
Hydrodynamic modelling
Non-photochemical quenching
Peter lake
Whole-lake manipulation

ABSTRACT

Adaptive physiological traits of cyanobacteria allow plasticity of responses to environmental change at multiple time scales. Most conventional phytoplankton models only simulate responses to current conditions without incorporating antecedent environmental history and adaptive physiological traits, thereby potentially missing mechanisms that influence dynamics. We developed an individual-based model (IBM) that incorporates information on light exposure history and cell physiology coupled with a hydrodynamic model that simulates mixing and transport. The combined model successfully simulated cyanobacterial growth and respiration in a whole-lake nutrient enrichment experiment in a temperate lake (Peter Lake, Michigan, USA). The model also incorporates non-photochemical quenching (NPQ) to improve simulations of cyanobacteria biomass based on validation against cyanobacteria cell counts and chlorophyll concentration. The IBM demonstrated that physical processes (stratification and mixing) significantly affect the dynamics of NPQ in cyanobacteria. Cyanobacteria had high fluorescence quenching and long photo-physiological relaxation periods during stratification, and low quenching and rapid relaxation in response to low light exposure history as the mixing layer deepened. This work demonstrates that coupling adaptive physiological trait with physical mixing into models can improve our understanding and enhance predictions of bloom occurrences in response to environmental changes.

1. Introduction

Non-photochemical quenching (NPQ) is an adaptive physiological trait used in cyanobacteria in response to high solar radiation. When light levels exceed cyanobacteria photosynthetic requirements, they can trigger NPQ to avoid photooxidative damage (Müller et al., 2001; Karapetyan, 2007). In aquatic environments, particularly at the water surface in daylight conditions, NPQ considerably reduces fluorescence yields (Bertone et al. 2018). Therefore, NPQ can lead to an incorrect interpretation of cyanobacterial biomass (Karapetyan, 2007), as it reduces fluorescence readings from *in situ* fluorometric probes (Rousso et al., 2021). NPQ consists of three distinct processes: energy-dependent NPQ (*qE*), state-transition quenching (*qT*), and photoinhibition quenching (*qI*) (Blommaert et al., 2017; Lucius et al., 2020). Each process has different relaxation kinetics, ranging from seconds to hours. *qE* relaxes or reverses within seconds, reducing fluorescence by up to 90 % through the generation of a pH gradient across the thylakoid membrane, linked to the xanthophyll cycle (Huot and Babin, 2010; Murchie and Lawson, 2013). *qT* involves the detachment of light-harvesting complex II (LHCII) from Photosystem II (PS II), which reduces photon absorption and total excitation energy, typically relaxing within 5 to 20 min after light exposure ends (Huot and Babin, 2010; Murchie and Lawson, 2013). *qI* is associated with photoinhibition and damage to D1 proteins in Reaction Centre II, preventing further photochemical reactions and taking several hours to relax (Müller et al., 2001; Morrison, 2003; Huot and Babin, 2010; Murchie and Lawson, 2013). These three processes are coupled and require joint consideration (Behrenfeld et al., 1998; Moore et al., 2006). Rousso et al. (2021) showed that prior light exposure influences the magnitude of NPQ and revealed a daily hysteresis pattern, with greater fluorescence suppression occurring in the afternoon

* Corresponding author at: Sir Samuel Griffith Centre (N78), Room 4.11, 170 Kessels Road, Nathan, Queensland 4111, Australia.
E-mail address: m.ranjbar@griffith.edu.au (M.H. Ranjbar).

https://doi.org/10.1016/j.ecolmodel.2024.110803
Received 22 April 2024; Received in revised form 14 June 2024; Accepted 10 July 2024
Available online 29 July 2024

compared to the morning for the same level of irradiance.

The light exposure history of cyanobacteria, which affects phycocyanin fluorescence and the estimation of cyanobacteria biomass by fluorometers, is affected by both surface light availability and physical processes in lakes. If turbulent mixing dominates over the average population floating velocity, there might be a limited time for high light exposure and the development of NPQ (Rousso et al., 2021; Ranjbar et al., 2022). Thus, phycocyanin output from a fluorometer near the water surface may provide a linear approximation of cyanobacteria biomass (Bertone et al., 2018). Conversely, if buoyant surface populations are not redistributed due to low rates of turbulent mixing, there exists the potential for substantial NPQ development, especially under high light levels (Rousso et al., 2021; Ranjbar et al., 2022); phycocyanin fluorescence will therefore be disconnected from biomass (Bertone et al., 2018). As such, understanding and prediction of NPQ and cyanobacteria biomass could be improved by accounting for the light exposure history of individuals and lake-scale physical processes (e.g., mixing). However, existing modelling approaches commonly fail to capture physiological responses of cyanobacteria to antecedent environmental conditions concurrently with physical processes in the water column, leading to inaccuracies in bloom predictions (Hellweger, 2017; Stow et al., 2022). These inaccuracies motivate the need for new lake-scale modelling approaches that incorporate the effects of antecedent conditions on cells (Xiao et al., 2022).

Individual-based models (IBMs) – sometimes referred to as agent-based models – can include the time history of processes that affect cyanobacterial bloom dynamics. Each bloom-forming element (e.g., cell or filament) in an IBM can carry a memory (e.g., of light exposure history). In IBMs, each individual has also a set of attributes and behaviors that are simulated as an individual entity influenced by environmental conditions, such that multiple individuals capture the intra-specific variability in cyanobacteria populations (Hellweger and Bucci, 2009; DeAngelis and Grimm, 2014). In addition, IBMs can be coupled to hydrodynamic models to capture the effects of stratification and mixing processes on the transport of cyanobacteria (Ranjbar et al., 2021). The first use of an IBM in ecology was in the 1970s using the JABOWA forest model (Botkin et al., 1972). However, the first IBM for cyanobacterial blooms was developed about three decades later by Wallace et al. (2000), who examined the relationship between *Microcystis* sp. buoyancy regulation and diurnal stratification. To date, IBMs have only occasionally been applied for cyanobacteria bloom modelling, mainly because of their complexity and high data and computational demands (Ranjbar et al., 2021).

In this study, for the first time, we modelled how cyanobacteria growth, respiration, NPQ, and entrainment/disentrainment interact to affect cyanobacteria biomass. For this purpose, we developed a novel IBM that was coupled to a hydrodynamic model. The model was applied to Peter Lake, Michigan, USA, in 2015, where a large bloom dominated by the cyanobacterium *Dolichospermum* sp. (comprising 93 % of the total community cell counts) occurred (Wilkinson et al., 2018). Therefore, the IBM was adapted to *Dolichospermum* sp. Nonetheless, the model is versatile and can also be adapted to the simulation of other bloom-forming buoyant cyanobacteria species. The model tracks the growth, light exposure history, and NPQ of each *Dolichospermum* filament as it is transported and mixed in three dimensions. We predicted that thermal stratification in a lake would lead to high daytime fluorescence quenching, followed by extended periods of photo-physiological relaxation, while mixing would cause low daytime quenching and rapid relaxation because of the low light exposure history of filaments. Testing this prediction requires a model able to consider the effects of NPQ on phycocyanin fluorescence measurements.

2. Methods

2.1. Study area

Peter Lake (Fig. 1) is a temperate lake (surface area = 2.7 ha, mean depth = 5.7 m, maximum depth = 18 m) located in Gogebic County, Michigan, USA (46.253° N, 89.504° W). The lake is oligotrophic to mesotrophic, and cyanobacterial blooms have not been observed in the lake except for periods of experimental fertilization (Buelo et al., 2022). Peter Lake lacks perennial inflow or outflow streams (Pace et al., 2021). A more detailed description of the study site can be found in Carpenter and Kitchell (1993).

In a whole-lake experiment conducted in 2015, inorganic nitrogen and phosphorus (20.3 mg N m^{-2} d^{-1} and 3.0 mg P m^{-2} d^{-1}; N:P molar ratio of 15:1) were added to the lake from day of year (DOY) 151 to 180 (i.e., 31 May to 29 June), resulting in a cyanobacterial bloom (Pace et al., 2017). Between DOY 175 and DOY 179, chlorophyll *a* concentration rose from approximately 23 to 40 μg L^{-1} after which it declined to approximately 18 μg L^{-1} on DOY 182 (Pace et al., 2017).

Microscopic counts revealed that cyanobacteria, primarily *Dolichospermum* sp., comprised 93 % of the phytoplankton biomass on DOY 180 (Wilkinson et al., 2018). In contrast, chrysophytes dominated the phytoplankton community on DOY 166 and 229, constituting approximately 45 % and 68 % of the total biomass, respectively (Wilkinson et al., 2018). A succession from chrysophytes to the cyanobacterium *Dolichospermum* appears to correspond to the fertilization event. The measured water temperature profiles show that the lake was more strongly stratified on DOY 180 compared to DOY 166 and 229. The interaction between stratification strength and the high ascent rate of *Dolichospermum* sp. (Carey et al., 2012; Visser et al., 2016) could in part explain its dominance on DOY 180. It is worth noting that in prior nutrient fertilization studies of Peter Lake, *Dolichospermum* also dominated (Cottingham et al., 1998). A plankton succession model (Cagle and Roelke, 2024) or an IBM incorporating different species and coupled with a hydrodynamic-ecological model would help us to better understand species succession and the occurrence of the *Dolichospermum* in Peter Lake in 2015.

The nutrient addition experiment caused a nutrient-replete condition (i.e., no nitrogen or phosphorus limitation) that led to high phytoplankton biomass in Peter Lake (Pace et al., 2017). Our model was applied to the period of DOY 175 to DOY 182 (i.e., 24 June to 1 July), when the lake experienced stratification, followed by mixing on DOY 181. This allowed us to assess the effectiveness of our IBM in capturing the impacts of both stratification and mixing conditions on the NPQ in cyanobacteria.

2.2. Hydrodynamic (lake) model

MIKE 3 Flow Model FM (DHI, 2021) was used for hydrodynamic modelling. The model is based on a numerical solution of the three-dimensional incompressible Reynolds Averaged Navier–Stokes equations, subject to the assumptions of Boussinesq and hydrostatic pressure. The horizontal eddy viscosity is estimated using the Smagorinsky formulation and the vertical eddy viscosity with the k-epsilon formulation. The model accounts for heat exchange between water and the atmosphere, calculated from latent and sensible heat flux, net shortwave, and net longwave radiation.

The spatial discretization is performed using a cell-centered finite volume method. For time integration, a semi-implicit approach is utilized, treating horizontal terms explicitly and vertical terms implicitly. Due to stability restrictions when using an explicit scheme, the time step interval must be selected so that the Courant-Friedrich-Lévy (CFL) number is less than one at all computational nodes. In MIKE 3 Flow Model FM, the time step for the hydrodynamic calculations is dynamic and determined to satisfy the mentioned stability criterion. In this study, the overall time step interval, which determines the frequency at which

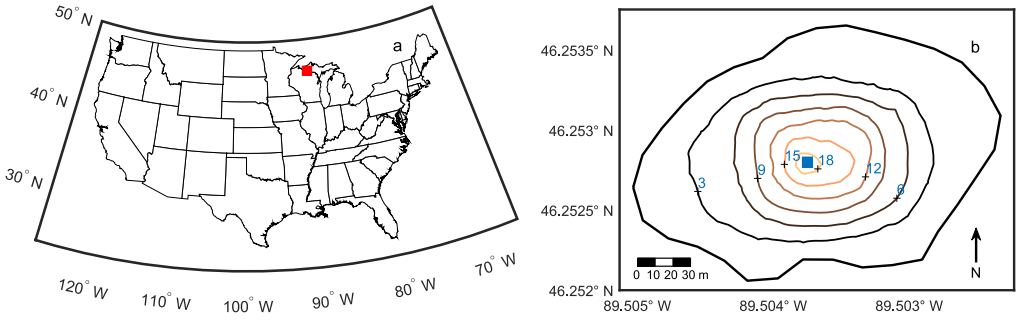

Fig. 1. Map of the USA and the location of Peter Lake is shown by the red inset (a). Bathymetry (m) of the lake and the location of the Peter Lake monitoring site is shown by the blue inset (b).

output can be obtained from the model, was set to one minute. Therefore, the hydrodynamic model produced one-minute output, including three-dimensional currents, water temperature, and turbulent diffusivity, as well as water level fluctuations. The model has been successfully used to simulate the hydrodynamic and thermal structure of inland water bodies (e.g., Sokolova et al., 2013; Zhang et al., 2020). The complete hydrodynamic model equations are available in the model's scientific documentation (DHI, 2021).

Xue et al. (2017) discussed the importance of three-dimensional lake models to adequately resolve horizontal and vertical mixing processes and reduce biases in lake surface temperature and thermal stratification. On this basis, we used a three-dimensional hydrodynamic model to simulate hydrodynamics in Peter Lake and drive the IBM. The model was driven by atmospheric forcings including air temperature, wind speed and direction, short and long wave radiation, precipitation, evaporation, and relative humidity. Air temperature and wind data were collected by a weather station deployed on a raft near the deepest point of Peter Lake (Fig. 1). Precipitation, evaporation, and short and long wave radiation data were obtained from the ERA5 reanalysis product available at a spatial resolution of 0.25°. Relative humidity was measured at the Noble F. Lee Municipal Airport at Woodruff, located ~40 km southwest of Peter Lake.

In the horizontal, the domain was configured with an unstructured triangular grid with a resolution varying from 20 m to 50 m. In the vertical, the three-dimensional domain comprised a combined sigma/z-level vertical distribution and vertical resolution was set to 0.05 m to enhance the representation of the vertical thermal structure, turbulent mixing, and consequently, the mixing and transport of *Dolichospermum* in the lake. A detailed description of model calibration is provided in Section 2.4.

2.3. Individual-based model (IBM)

The IBM was developed in the MIKE ABM Lab environment (DHI 2021). The time step in the IBM was set to one minute. The length of the simulation was one week, between the DOY 175 and DOY 182 in 2015. At the beginning of the simulation, filaments were released between a depth of 1.2 m and 1.3 m with a biomass of 13.81 pg C. At one-minute intervals, the IMB was forced with simulated hydrodynamic model outputs (i.e., three-dimensional currents, water temperature, and turbulent diffusivity, as well as water level fluctuations) in a manner similar to that of Ani et al. (2024). During each time step, *Dolichospermum* filaments were subjected to the local environmental conditions, accrued or lost biomass based on the balance between the photosynthesis and respiration of filaments, and experienced light-induced fluorescence quenching.

The lake environment was configured with unstructured triangular grids for setting the hydrodynamic model domain. The computational domain was the same for both the hydrodynamic model and IBM. The filaments were able to move between grid cells in the model domain, changing position according to their floating velocity and advection and dispersion processes in the lake.

The IBM was developed to capture the interaction between physiological traits and physical processes controlling the dynamics of the *Dolichospermum* bloom. Adaptive physiological traits were incorporated into the IBM. The main adaptive trait was the response of the filaments to light exposure history. Prior light exposure was incorporated into the IBM, enabling the model to replicate the pattern of hysteresis observed in NPQ dynamics in cyanobacteria, showing greater fluorescence suppression in the afternoon compared to the morning for the same level of irradiance (Rousso et al., 2021). In addition, the coupled IBM-hydrodynamic model considered lake-scale processes (e.g., three-dimensional mixing of cyanobacteria).

The main outputs of the IBM were the distribution of filaments, biomass, and NPQ of *Dolichospermum*. A random walk technique (Visser, 1997) was used to capture the effects of sub-grid scale turbulent diffusion on the trajectories of filaments, which helped to avoid the purely deterministic and numerical synchronization effects.

Due to the complexity and high computational demand of IBMs (Hellweger et al., 2016), it was not feasible to simulate each individual cell that contributed to the bloom (e.g., the maximum number of *Dolichospermum* cells in Peter Lake in 2015 exceeded 2.0×10^5 cells m L^{-1}). To overcome this limitation, super individual-based modelling was used, where a "super individual" represents a collection of numerous individuals, with the number of individuals represented determined by an upscaling factor (Scheffer et al., 1995; Hellweger et al., 2016). In this study, the upscaling factor was 4.09×10^{12} throughout the simulation period. The number of super-individuals was 100 during the simulation period, and changes in the modelled biomass were attributed to variations in the filament size, which was one of the model outputs.

2.3.1. Submodels of the IBM

2.3.1.1. Growth and respiration submodel. Model equations are given as follows. Table 1 lists model parameters and state variables. In the IBM, the maximum daily growth rate (μ_{max}) of filaments was size-dependent, with positive growth rate led to filament elongation and vice versa for negative growth rate. The maximum growth rate of each filament at 20 °C was determined based on the ratio of its surface area (s in μm^2) to volume (v in μm^3) (Reynolds, 1989) as:

$$\mu_{max} = 1.142\left(sv^{-1}\right)^{0.325} \quad (1)$$

The net daily growth rate (μ_{net}) was governed by the following equation:

$$\mu_{net} = \mu_{max} L_T L_L - \mu_R \quad (2)$$

where L_T and L_L are limitation terms applied to regulate growth dependence on water temperature (T) and light (L) that a filament experienced, respectively, and μ_R (d^{-1}) is the respiration rate, which was

Table 1
Model parameters and state variables used in the study.

Description	Unit	Value
Roughness height	m	5.0×10^{-2}
Drag coefficient	Unitless	1.255×10^{-3}
Constant in Dalton's law	Unitless	5.0×10^{-1}
Wind coefficient in Dalton's law	Unitless	9.0×10^{-1}
Critical wind speed for latent heat flux	m s^{-1}	2
Transfer coefficient for heating	Unitless	1.10×10^{-3}
Transfer coefficient for cooling	Unitless	6.25×10^{-3}
Critical wind speed for sensible heat flux	m s^{-1}	3.7
Beta in Beer's law	Unitless	6.0×10^{-1}
Light extinction coefficient	m^{-1}	1.4–1.7
Maximum vertical eddy viscosity	m^2 s^{-1}	1.0×10^{-6}
R, term representing the effects of respiration/mortality at 20 °C	d^{-1}	1.0×10^{-1}
θ, respiration/mortality coefficient	Unitless	1.1
T^0, optimum temperature	°C	22
q, thermal dispersion parameter	°C	5
e, irradiance half-saturation constant	µmol m^{-2} s^{-1}	114.25
u, irradiance inhibition constant	m^2 s µmol^{-1}	2.19×10^{-4}
PRR, photosynthesis recovery rate from NPQ	µmol m^{-2} s^{-1}	800
α, NPQ calibration coefficient	Unitless	1.2×10^{-2}
Filaments velocity	m d^{-1}	1
Minimum cell biomass	pg C cell^{-1}	13.81
Chlorophyll a content per cell	pg cell^{-1}	1.65

estimated as:

$$\mu_R = R\theta^{(T-20)} \tag{3}$$

where R is a term for the combined effects of respiration and mortality at 20 °C, and θ is a coefficient governing the respiration/mortality response to water temperature. R and θ were set to 0.1 d^{-1} and 1.1, respectively (Ranjbar et al., 2022). The temperature limitation term was given by (Prokopkin et al., 2006):

$$L_T = \exp\left(-\left(\frac{T - T^0}{q}\right)^2 \right) \tag{4}$$

where T^0 is the optimum temperature, and q is the thermal dispersion parameter. T^0 and q were set to 22 °C and 5 °C, respectively (Hellweger et al., 2008). The light limitation term was governed by the following equation (Prokopkin et al., 2006):

$$L_L = \frac{I_z}{I_z + e + uI_z^2} \tag{5}$$

where I_z is the irradiance that a filament was exposed to at depth z, e (µmol m^{-2} s^{-1}) is the half-saturation constant, and u (m^2 s µmol^{-1}) is the inhibition constant. The parameters e and u were set to 114.25 µmol m^{-2} s^{-1} and 2.19×10^{-4} m^2 s µmol^{-1}, respectively (Hellweger et al., 2008). I_z was estimated by Lambert-Beer's law of exponential light extinction:

$$I_z = I_0 \exp(-K_d z) \tag{6}$$

where I_0 (W m^{-2}) is the surface irradiance, and K_d (m^{-1}) is the light extinction coefficient. I_0 and K_d were determined based on photosynthetically active radiation (PAR) measured on Peter Lake and in the water column, respectively. To remove the effect of transient clouds on surface PAR, the 60-minute moving average of PAR was used. Based on μ_{net}, the doubling time (D_{time}), and filament size changes ($D_{G,t}$) at the current time step (t), were calculated as:

$$D_{time} = \frac{\ln(2)}{\mu_{net}} \tag{7}$$

$$D_{G,t} = D_{t-1} \times 2^{\frac{\Delta t}{D_{time}}} \tag{8}$$

where D_{t-1} is the filament size at the previous time step $(t-1)$ and Δt is the time interval.

2.3.1.2. Non-photochemical quenching (NPQ) submodel. Experimental results of Rousso et al. (2021) were used to determine the light-induced fluorescence quenching in *Dolichospermum* in the IBM. Since light exposure history affects the magnitude of NPQ (Rousso et al., 2021), we aimed to develop a representation of NPQ which considers the cumulative irradiance instead of instantaneous irradiance. The cumulative light dose with a built-in recovery was calculated as:

$$CL_t = \max(IL_t - PRR + CL_{t-1}, 0) \tag{9}$$

where CL_t and CL_{t-1} (µmol m^{-2} s^{-1}) are the cumulative light dose at the current and previous time steps, respectively. IL_t (µmol m^{-2} s^{-1}) is the instantaneous light dose at the current time step, and PRR is the photosynthesis recovery rate from NPQ. The light-induced variability in phycocyanin fluorescence observed in Rousso et al. (2021) was plotted against CL calculated using Eq. (9) (Fig. 2a). The rate of NPQ ($d_{NPQ,t}$) was plotted against CL, and a linear trendline was fitted to the data points (Fig. 2b). The equation of the trendline was used as $d_{NPQ,t}$ in the IBM:

$$d_{NPQ,t} = \alpha\left(-3.0 \times 10^{-6} CL_t + 0.3 \right) \tag{10}$$

where α is the calibration coefficient. Based on $d_{NPQ,t}$, NPQ at the current time step (NPQ_t) was calculated as:

$$NPQ_t = NPQ_{t-1} + d_{NPQ,t} \tag{11}$$

In the IBM, NPQ_t range was limited between zero and 90 % (Roesler and Barnard, 2013) and was set to zero when CL_t was zero.

2.3.1.3. Buoyancy and transport submodel. In line with Hellweger et al. (2008), the floating velocity of filaments was set to 1.0 m d^{-1}. The transport of each filament depends on the interaction between its floating velocity and advection and dispersion processes as discussed by Ranjbar et al. (2021). The flow field and turbulent diffusivity derived from the hydrodynamic model were used to capture the advection and dispersion of filaments.

2.4. Model evaluation

In situ water temperature profiles, collected using a thermistor chain spanning depths from 0.5 to 5 m near the center of Peter Lake (Coloso et al., 2011), were used to assess the model's ability to simulate the hydrodynamics in the lake. For evaluation of the hydrodynamic model, time series of measured and modelled Schmidt stability (S_t; Idso, 1973) were also compared. Based on vertical water temperature profiles, S_t denotes the energy required to fully mix the water column. The "Lake Analyzer" tool was used for the calculation of S_t (Read et al., 2011).

To calibrate the hydrodynamic model, the transfer coefficient for cooling, affecting the convective heat transfer between the water and the atmosphere, and the Beta coefficient in Beer's Law that determines the short-wave penetration into the water were set to 0.00625 and 0.6, respectively (note that the light extinction coefficient (K_d) varied between 1.4 and 1.7 m^{-1} based on PAR profiles). The minimum wind speed used for the calculation of the convection flux is determined as the larger value between the wind speed at the open boundary and the critical wind speed. The default value for the critical wind speed is 2 m s^{-1}, but in this study, it was set to 3.7 m s^{-1}. Furthermore, the maximum vertical eddy viscosity was set to 1.0×10^{-6} m^2 s^{-1}, which is consistent with values for a small, forested lake (Chapra, 2008; Zhao et al., 2021). The results of the modelled temperature profiles and vertical distribution of cyanobacteria (i.e., accumulation of cyanobacteria during the stratification period and their redistribution during the mixing event) showed that the modelled vertical eddy viscosity was sufficiently accurate to capture the vertical mixing processes given the difficulty in

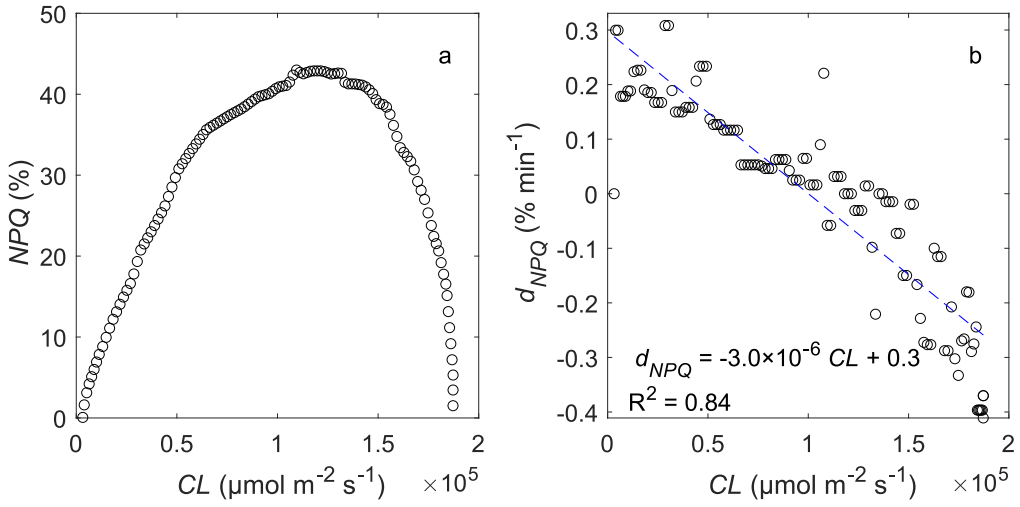

Fig. 2. Non-photochemical quenching (*NPQ*) observed by Rousso et al. (2021) (a) and rate of *NPQ* (d_{NPQ}) versus cumulative light dose (*CL*), including recovery from NPQ (b). The equation for best-fit line and the R-squared value are shown in (b). Based on the observed *NPQ* dynamics in *Dolichospermum* (a), d_{NPQ} in the IBM was calculated (b). Positive d_{NPQ} represents NPQ development, while negative d_{NPQ} represents NPQ relaxation in response to accumulated light exposure.

quantifying turbulence for a hydrostatic model (for more details see Hodges et al., 2000; Rueda and MacIntyre, 2010).

The IBM was calibrated against *Dolichospermum* cell counts, which were estimated from a relationship between the microscopic cyanobacteria counts and phycocyanin sensor readings at a depth of 0.75 m. Phycocyanin was measured using a YSI 6600V2-4 multiparameter sonde (Yellow Springs Instruments, Yellow Springs, Ohio, USA). The microscopic counts were done on samples from DOY 145, 166, 180, and 229. To obtain reasonable estimates of cell counts, phycocyanin readings on DOY 180 were corrected to remove the influence of NPQ. Based on the modelled fluorescence suppression, the NPQ correction factor and NPQ-corrected phycocyanin readings were determined. The raw phycocyanin readings (i.e., NPQ-impacted phycocyanin readings) were calibrated with the correction factor to obtain corrected phycocyanin readings (i.e., NPQ-corrected phycocyanin readings). The total biovolume of *Dolichospermum* (*BV*) was then correlated with the maximum phycocyanin readings (*PC*) on DOY 145, 166, 180, and 229, and the following equation was obtained:

$$BV = 4.70 \times 10^{-5} PC + 0.083 \quad (12)$$

Subsequently, *Dolichospermum* cell counts were calculated based on the biovolume, in line with Rousso et al. (2022). Note that phycocyanin readings on DOY 145, 166, and 229 were not corrected. Water-column stability was high on DOY 180 (St = 163 J m^{-2}), and filaments accumulated near the water surface and experienced a high level of light, leading to a significant NPQ. As a result, it was necessary to correct phycocyanin readings on DOY 180 to remove the influence of NPQ and obtain reasonable estimates of cell counts. In comparison with DOY 180, water-column stability was lower on DOY 145 and 166 with *St* of approximately 78 and 119 J m^{-2}, respectively. *St* on DOY 229 was about 188 J m^{-2}, but there was mixing between DOY 228 and 233 that reduced *St* from 200 to 132 J m^{-2}. Therefore, we assumed that filaments were redistributed on DOY 145, 166, and 229 and received lower light than DOY 180. As a result, it is reasonable to consider a linear relationship between phycocyanin readings and biomass on those days.

Modelled *Dolichospermum* cell counts were determined based on the number of filaments and constituent cells in the top 0.75-m layer of the lake at each time step, and the number of constituent cells of each filament was calculated by dividing the total filament biomass by the minimum cell biomass (13.81 pg C cell^{-1}). To match the estimated and simulated *Dolichospermum* cell counts, *PRR* in Eq. (9) and α in Eq. (10) were set to 800 μmol m^{-2} s^{-1} and 0.012, respectively.

To show the ability of the model to reproduce the observed cyanobacteria biomass, the IBM was also calibrated against the chlorophyll *a* grab samples collected each day near the deepest point of Peter Lake at a depth of 0.5 m. The modelled chlorophyll *a* was calculated based on the chlorophyll *a* content per cell and the number of cells in the top 0.5-m layer of the lake at each time step. To obtain the best agreement between model results and field data, chlorophyll *a* content per cell was set to 1.65 pg cell^{-1} in the IBM.

To assess the performance of the model, mean relative absolute error (MRAE) and correlation coefficient (r) were used. The MRAE was calculated as:

$$MRAE = \frac{1}{n}\sum_{i=1}^{n}\frac{|y_i - \widehat{y_i}|}{\widehat{y_i}} \quad (13)$$

where n is the number of observations. y_i and $\widehat{y_i}$ are simulated and observed data, respectively.

3. Results

3.1. Hydrodynamic model results

From DOY 175 to 179, the water column was thermally-stratified, and Schmidt stability (S_t) increased by about 30 J m^{-2}. Then, the water column was partially mixed, and S_t decreased from 168.6 J m^{-2} to 130 J m^{-2} by DOY 182 (Figs. 3 and 4b). Surface water temperature and S_t also exhibited diel variations mainly in response to convective heating and cooling (Figs. 3 and 4b). As observed in Fig. 4 and Table 2, the hydrodynamic model accurately reproduced the thermal structure and S_t under stratified and mixing conditions. Correlation coefficients of 0.997 for water temperature and 0.91 for S_t were noted between model results and observations. Furthermore, an MRAE of 3.6 % and 2.8 %, pertaining to water temperature and S_t, respectively, was obtained.

3.2. IBM results

During the period of stratification, near-surface *Dolichospermum* cell counts and chlorophyll *a* concentration increased, but subsequently decreased, which coincided with the mixing event (Fig. 5). PAR measured by a weather station deployed on a raft near the deepest point of Peter Lake varied modestly during the study period (Fig. 5a). Similarly, the average instantaneous light (*IL*) dose experienced by filaments in the top 0.75-m layer of the lake showed modest variability (Fig. 5b).

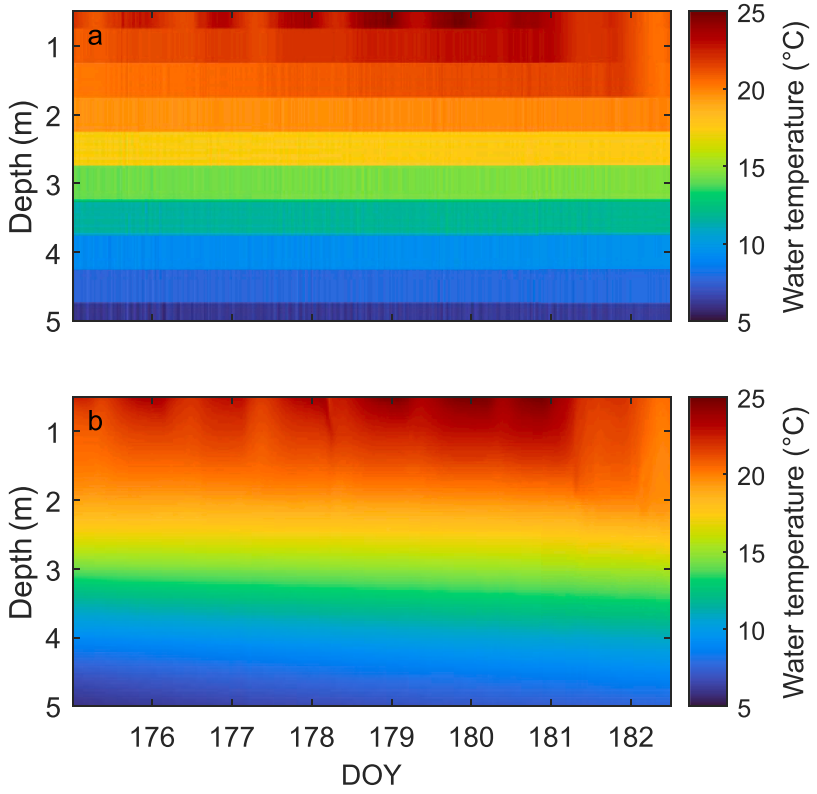

Fig. 3. Measured (a) and modelled (b) water temperature in Peter Lake in 2015 for the upper 5 m of the water column. Water temperature was measured by a thermistor chain with a vertical resolution of 0.5 m (water temperature at depth of 4.5 m was determined by averaging the values of water temperature at depths 4 and 5 m). The simulated water temperature profile (b) had a vertical resolution of 0.05 m, in line with the vertical resolution of the hydrodynamic model.

However, the cumulative light (*CL*) dose encountered by the filaments was significantly higher during the stratification period (DOY 175–179) than during the mixing period (DOY 181–182) when filaments were entrained and mixed more deeply (Fig. 5c). Low surface PAR on DOY 180 (Fig. 5a) led to filaments experiencing a low light dose (Fig. 5b,c).

Estimated *Dolichospermum* cell counts exceeded 2.0×10^5 cells mL^{-1} and then decreased to around 6.4×10^3 cells mL^{-1} over DOY 175 to 182 (Fig. 5d). As observed in Fig. 5d and Table 2, modelled NPQ-impacted *Dolichospermum* cell counts were highly correlated with observations ($r = 0.78$, MRAE = 19.7 %). Fig. 5d also shows the variation in the NPQ-free *Dolichospermum* cell counts. The maximum difference between NPQ-impacted and NPQ-free cell counts occurred around noon due to high NPQ (Fig. 5d). As seen in Fig. 5d and Table 2, the agreement between the *in situ* fluorometry and modelled NPQ-free cell counts ($r = 0.59$, MRAE = 32.1 %) was lower than that between the *in situ* fluorometry and modelled NPQ-impacted cell counts ($r = 0.78$, MRAE = 19.7 %). Therefore, incorporating NPQ into the IBM improved the model predictions. NPQ was higher during stratification when NPQ relaxation kinetics did not compensate for high light exposure (Fig. 5e). The NPQ relaxation duration was shorter during the mixing event due to the lower light exposure and relatively low NPQ (Fig. 5e).

Between DOY 175 and 179, chlorophyll *a* concentration rose from approximately 23 to 40 μg L^{-1} after which it declined to approximately 18 μg L^{-1} on DOY 182 (Fig. 5f). There is a good agreement between daily manual chlorophyll *a* samples and modelled chlorophyll *a* with a correlation coefficient of 0.8 and an MRAE of 16.6 % at the time of grab sampling in the mornings (Fig. 5f and Table 2).

Fig. 6 shows spaghetti plots of filament vertical distribution, *IL*, *CL*, and *NPQ* at the individual level. Most filaments accumulated near the water surface during the stratification period (Fig. 6a). As a result, they experienced a higher level of instantaneous and cumulative light (Fig. 6b, c), leading to more significant NPQ during the stratification (Fig. 6d). However, the mixing event redistributed the filaments to deeper depths (Fig. 6a). Therefore, the filaments encountered lower light (Fig. 6b, c) and, in turn, lower NPQ with a shorter relaxation duration (Fig. 6d).

4. Discussion and conclusions

We developed a dynamic, mechanistic IBM of *Dolichospermum* focusing on adaptive physiological traits of cyanobacteria in response to current and antecedent environmental conditions. In this study, the effect of NPQ was removed from fluorometric probe readings to distinguish between observed fluorescence and cyanobacteria biomass, which is not possible with conventional cyanobacterial bloom models.

Variability in cyanobacteria cell counts observed by fluorescence probes is not only driven by changes in biomass but also other artefacts arising from complex interactions among growth and loss, NPQ, and entrainment/disentrainment processes. When thermal stratification occurred in Peter Lake and S_t increased, the filaments were exposed to high levels of solar radiation in the near-surface region because their vertical flotation velocity dominated over redistribution from turbulent mixing. This accumulation in the illuminated and warm uppermost layers increased cyanobacteria growth rates, leading to higher biomass near the water surface. In addition, this accumulation led to higher levels of NPQ, and the linear relationship between fluorescence and cyanobacterial biomass was no longer valid. The growth resulted in a net increase in *Dolichospermum* cells, however, denoted by increased fluorescence in night-time observations (i.e., when NPQ relaxation had been complete). After this growth period, mixing caused the filaments to be redistributed away from the surface and decreased the near-surface biomass. This redistribution also prevented sustained exposure of cyanobacteria to high surface irradiances (MacIntyre, 1993) which reduced NPQ, but also limited growth through light limitation (cf. Visser et al., 2016).

The model results show that the relationship between cyanobacteria

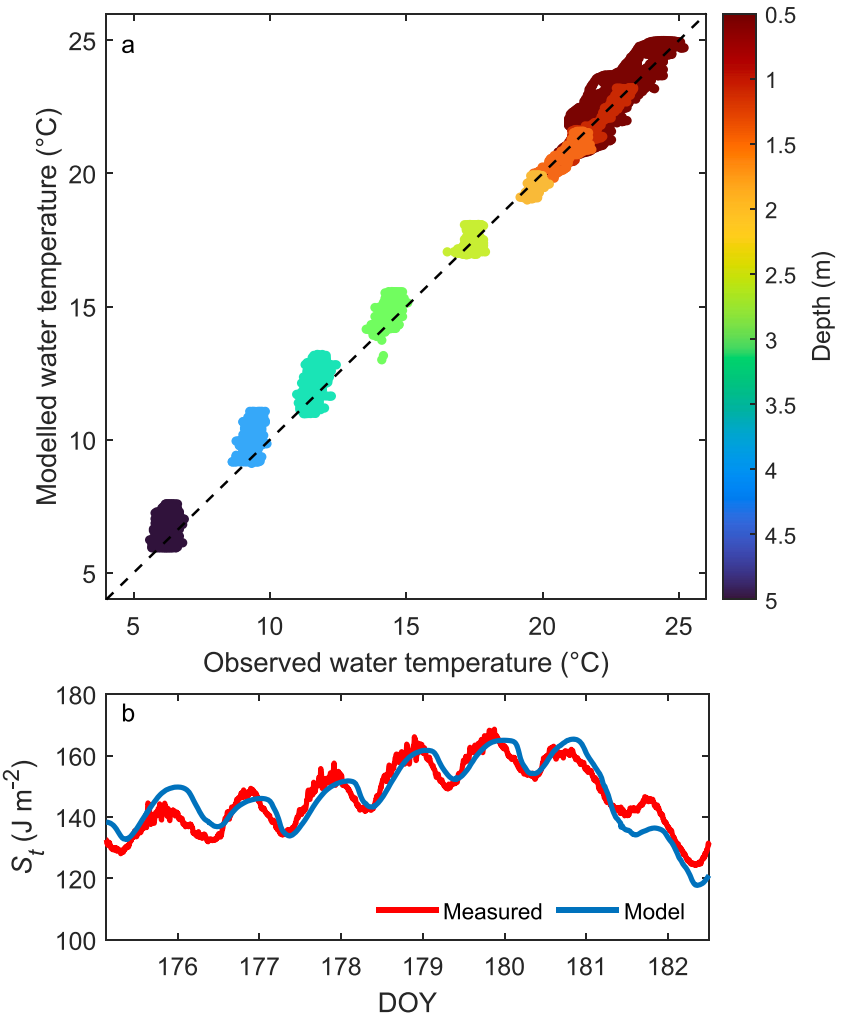

Fig. 4. Comparison of simulated and measured water temperatures (a) and Schmidt stability (S_t) (b) in Peter Lake in 2015. The dashed line in (a) corresponds to the 1:1 line. S_t was calculated based on water temperature profiles.

Table 2
Goodness-of-fit metrics (correlation coefficient, *r*, and mean relative absolute error, MRAE) for water temperature, Schmidt stability (S_t), chlorophyll *a*, and *Dolichospermum* cell counts.

Model	Variable	*r*	MRAE (%)
Lake model	Water temperature	0.997	3.6
Lake model	S_t	0.910	2.8
IBM	Chlorophyll *a*	0.800	16.6
IBM with NPQ	*Dolichospermum* cell counts	0.780	19.7
IBM without NPQ	*Dolichospermum* cell counts	0.590	32.1

blooms and water column stability in lakes is crucial in understanding the dynamics of these blooms. According to the model results, when water-column stability is high, cyanobacteria can disentrain from the turbulence and accumulate near the water surface, consistent with the observations by Humphries and Imberger (1982) and Hozumi et al. (2020). The accumulation of cyanobacteria near the water surface promotes their growth, as they can experience higher temperatures and light levels (Hozumi et al., 2020). Climate change is expected to have a profound effect on the stratification and mixing regimes of lakes (Woolway and Merchant, 2019), with significant consequences for bloom dynamics (Carey et al., 2012). In dimictic lakes, like Peter Lake, which typically undergo seasonal mixing in spring and autumn while stratifying continuously during the warmer months in between, climate change can result in prolonged stratification periods and elevated water temperatures during the summer months (Shatwell et al., 2019). Some dimictic lakes are projected to become predominantly monomictic lakes, characterized by seasonal mixing only in winter (Ficker et al., 2017; Shatwell et al., 2019; Woolway and Merchant, 2019). The prolonged stratification can provide an extended period during which cyanobacteria can benefit from buoyancy.

The early cyanobacterial bloom IBM work by Wallace et al. (2000), who examined the relationship between cyanobacteria buoyancy and the daily stratification/destratification cycle, set a foundation for the buoyancy and transport submodel of our IBM. Furthermore, the growth and respiration submodel of the IBM was developed in line with the prior literature (e.g., Hellweger et al., 2008). In addition, lake-scale processes (e.g., three-dimensional mixing of cyanobacteria) were incorporated into the IBM to enhance its predictive capability for lake-scale responses (Stow et al., 2022). The novelty of this study lies in the incorporation of responses of adaptive physiological traits of cyanobacteria to light history. Most previously published studies were restricted to models in which state variables responded directly to exogenous factors only at the current time step, thus preventing the simulation of emergent physiological features of cyanobacteria, as discussed by Hamilton et al. (2021). Our IBM was adapted for *Dolichospermum* sp., but it can take into account various traits of different strains and species. Therefore, the model has the capability to capture the intra- and interspecific variations and community structure of phytoplankton, providing insight into why certain species are found under certain environmental conditions (Litchman et al., 2010) and

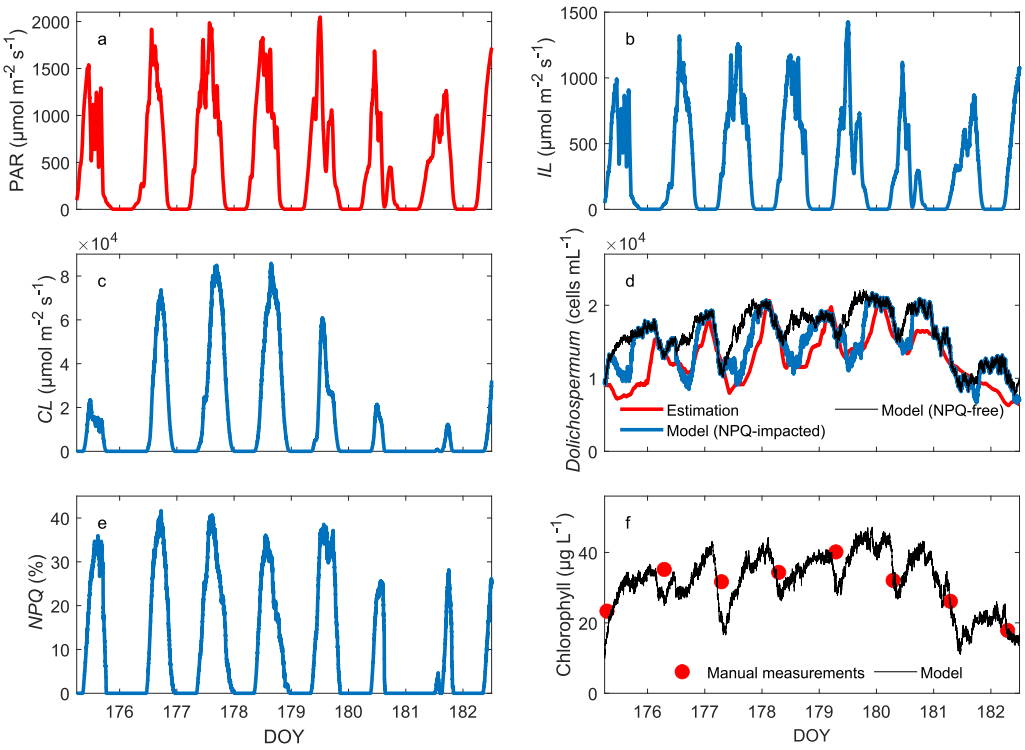

Fig. 5. Variations in surface PAR (a), instantaneous light dose (*IL*) (b), and cumulative light dose (*CL*) (c), and comparison between modelled and 3-h moving average of estimated *Dolichospermum* cell counts in the top 0.75-m layer of Peter Lake in 2015 (d). Non-photochemical quenching (*NPQ*) is shown in (e). A comparison between daily manual chlorophyll *a* samples and modelled chlorophyll *a* in the top 0.5-m layer is presented in (f). The curves in (b), (c), and (e) are the average *IL, CL*, and *NPQ* that filaments in the top 0.75-m layer of the lake experienced at each time step. The red line in (d) shows *Dolichospermum* cell counts from *in situ* fluorometry.

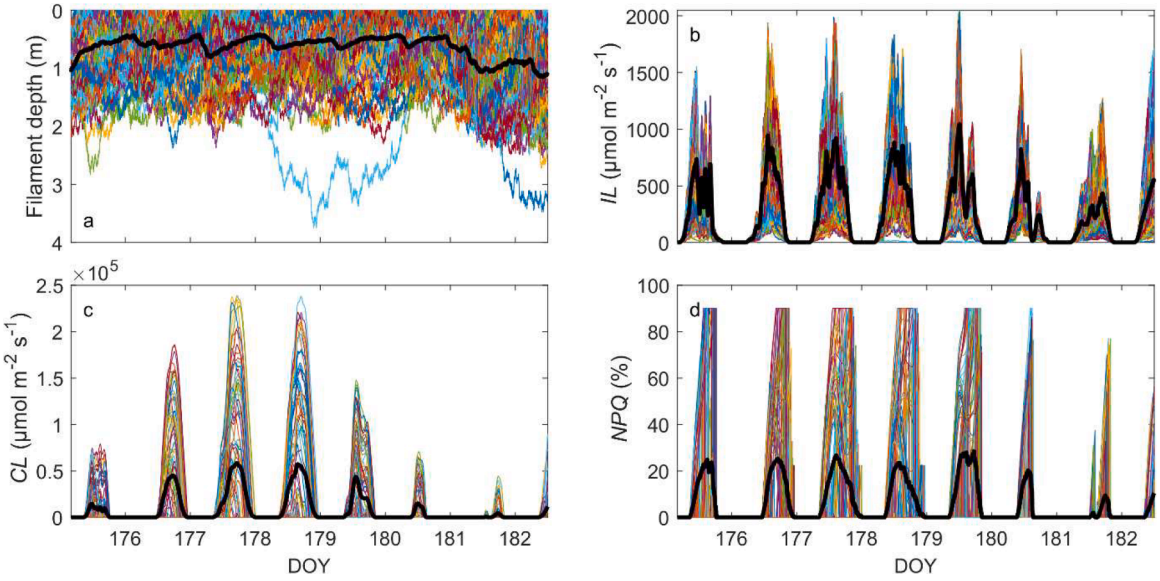

Fig. 6. Variations in depth of individual *Dolichospermum* filaments (multiple colours) (a), instantaneous light dose (*IL*) (b), cumulative light dose (*CL*) (c), and non-photochemical quenching (*NPQ*) (d) experienced by the filaments in Peter Lake in 2015. The thick black lines represent mean values at each time step. *NPQ* range was limited between zero and 90 % in line with Roesler and Barnard (2013).

advancing community predictions under climate change conditions. The IBM model is also a step towards improving mechanistic understanding of growth limitation and provides further opportunity to dynamically model cell quotas at the individual level.

The IBM enabled the study of adaptive physiological traits in a way that has not been possible using conventional models or statistical techniques. The model depicted the effects of antecedent conditions experienced by individuals on bloom dynamics and led to more accurate predictions of dynamics. In conventional approaches, bloom-forming colonies or filaments are often modelled as chemical molecules (i.e., pigments are equated to colonies\filaments) and average properties of a population within a control volume are simulated (Hellweger and

Kianirad, 2007). In statistical techniques, relationships between input and response variables are used for hindcasts and near-term forecasts of cyanobacterial blooms (Ralston and Moore, 2020). The key departure of our model from other cyanobacteria models is its ability to incorporate antecedent environmental history and adaptive physiological traits. The IBM captured the light exposure history to resolve the dynamics of fluorescence suppression and NPQ relaxation kinetics. With sustained high light exposure during stratification, light-induced fluorescence suppression was severe and NPQ relaxation kinetics were slow. Fluorescence suppression was reduced, and NPQ relaxation occurred quickly under fluctuating light experienced by cyanobacteria during vertical mixing. NPQ can be relaxed within seconds to hours (Müller et al., 2001; Huot and Babin, 2010). Quenching associated with photoinhibition can take several hours as cells repair their photosynthetic apparatus (Müller et al., 2001; Huot and Babin, 2010). In addition to capturing NPQ relaxation kinetics, quantitative NPQ estimates from the model allow distinction from temporal changes in phytoplankton biomass caused by vertical mixing or growth. Thus, the IBM can be used to deconvolve the cyanobacteria biomass variability driven by physical processes from that driven by physiological processes. The universality of light-induced quenching and the widespread use of fluorescence probes to estimate cyanobacterial biomass in surface waters highlight the value of the IBM for a better prediction of cyanobacterial bloom dynamics in lakes and reservoirs worldwide.

In conclusion, the development of a mechanistic IBM for cyanobacterial bloom prediction in this study advanced our understanding of adaptive physiological traits and antecedent environmental influences on cyanobacterial blooms. Developing IBMs for understanding and predicting cyanobacterial blooms is a promising area of research with major implications for bloom management.

CRediT authorship contribution statement

Mohammad Hassan Ranjbar: Writing – original draft, Visualization, Validation, Software, Methodology, Conceptualization. **David P. Hamilton:** Writing – review & editing, Supervision, Methodology, Conceptualization. **Michael L. Pace:** Writing – review & editing, Methodology, Data curation. **Amir Etemad-Shahidi:** Writing – review & editing, Supervision, Methodology. **Cayelan C. Carey:** Writing – review & editing, Methodology. **Fernanda Helfer:** Writing – review & editing, Supervision, Methodology.

Declaration of competing interest

The authors declare that they have no known competing financial interests or personal relationships that could have appeared to influence the work reported in this paper.

Data availability

The data used in this study are available in the North Temperate Lakes Long-Term Ecological Research database (http://lter.limnology.wisc.edu) and on Zenodo (http://doi.org/10.5281/zenodo.10648324). The individual-based model was developed based on MIKE ECO Lab (https://www.mikepoweredbydhi.com/products/mike-eco-lab).

Acknowledgments

This work was supported by a Griffith University International Postgraduate Research Scholarship and Griffith University Postgraduate Research Scholarship received by MHR. Support is acknowledged from the Australian Research Council to DPH (DP190101848) for 'Next-generation models to predict cyanobacteria harmful algal blooms' and to DPH and MHR (DP240100269) for 'A paradigm shift for predictions of freshwater harmful cyanobacteria blooms'. NSF grant DEB 1754712 to MLP is also acknowledged. CCC, DPH, and MHR were supported by NSF grants 2318862 and 2330211. Support from the US-Australian Fulbright Commission to CCC is also acknowledged. We thank the Cascade project who collected and organized the data used in this paper. We also thank DHI for providing the academic license for the MIKE model.

References

Ani, C.J., Baird, M., Robson, B., 2024. Modelling buoyancy-driven vertical movement of *Trichodesmium* application in the Great Barrier Reef. Ecol. Modell. 487, 110567.
Behrenfeld, M.J., Prasil, O., Kolber, Z.S., Babin, M., Falkowski, P.G., 1998. Compensatory changes in photosystem II electron turnover rates protect photosynthesis from photoinhibition. Photosyn. Res. 58 (3), 259–268.
Bertone, E., Burford, M.A., Hamilton, D.P., 2018. Fluorescence probes for real-time remote cyanobacteria monitoring: a review of challenges and opportunities. Water Res. 141, 152–162.
Blommaert, L., Huysman, M.J., Vyverman, W., Lavaud, J., Sabbe, K., 2017. Contrasting NPQ dynamics and xanthophyll cycling in a motile and a non-motile intertidal benthic diatom. Limnol. Oceanogr. 62 (4), 1466–1479.
Botkin, D.B., Janak, J.F., Wallis, J.R., 1972. Some ecological consequences of a computer model of forest growth. J. Ecol. 849–872.
Buelo, C., Pace, M., Carpenter, S., Stanley, E., Ortiz, D., Ha, D., 2022. Evaluating the performance of temporal and spatial early warning statistics of algal blooms. Ecol. Appl. 32 (5), e2616.
Cagle, S.E., Roelke, D.L., 2024. Chaotic mixotroph dynamics arise with nutrient loading: implications for mixotrophy as a harmful bloom forming mechanism. Ecol. Modell. 492, 110714.
Carey, C.C., Ibelings, B.W., Hoffmann, E.P., Hamilton, D.P., Brookes, J.D., 2012. Eco-physiological adaptations that favour freshwater cyanobacteria in a changing climate. Water Res. 46 (5), 1394–1407.
Carpenter, S.R., Kitchell, J.F., 1993. Primary Production and Its Interactions with Nutrients and Light Transmission. The Trophic Cascade in Lakes. Cambridge University Press, pp. 225–251.
Chapra, S.C., 2008. Surface Water-Quality Modeling. Waveland Press.
Coloso, J.J., Cole, J.J., Pace, M.L., 2011. Short-term variation in thermal stratification complicates estimation of lake metabolism. Aquat. Sci. 73, 305–315.
Cottingham, K.L., Carpenter, S.R., Amand, A.L.S., 1998. Responses of epilimnetic phytoplankton to experimental nutrient enrichment in three small seepage lakes. J. Plankton Res. 20 (10), 1889–1914.
DeAngelis, D.L., Grimm, V., 2014. Individual-based models in ecology after four decades. F1000 Prime Rep. 6 (39), PMC4047944.
DHI, 2021. MIKE 3 Flow Model FM, Scientific Documentation. DHI Water & Environment.
Ficker, H., Luger, M., Gassner, H., 2017. From dimictic to monomictic: empirical evidence of thermal regime transitions in three deep alpine lakes in Austria induced by climate change. Freshw. Biol. 62 (8), 1335–1345.
Hamilton, D.P., Anderson, C.R., Hense, I., Chapra, S.C., 2021. Future perspectives in modeling harmful algal bloom (HAB) responses to climate change: guidelines for HABs modeling. Guidelines for the Study of Climate Change Effects on HABs 104–120. UNESCO-IOC/SCOR.
Hellweger, F.L., 2017. 75 years since Monod: it is time to increase the complexity of our predictive ecosystem models (opinion). Ecol. Modell. 346, 77–87.
Hellweger, F.L., Bucci, V., 2009. A bunch of tiny individuals—individual-based modeling for microbes. Ecol. Modell. 220 (1), 8–22.
Hellweger, F.L., Clegg, R.J., Clark, J.R., Plugge, C.M., Kreft, J.U., 2016. Advancing microbial sciences by individual-based modelling. Nat. Rev. Microbiol. 14 (7), 461–471.
Hellweger, F.L., Kianirad, E., 2007. Individual-based modeling of phytoplankton: evaluating approaches for applying the cell quota model. J. Theor. Biol. 249 (3), 554–565.
Hellweger, F.L., Kravchuk, E.S., Novotny, V., Gladyshev, M.I., 2008. Agent-based modeling of the complex life cycle of a cyanobacterium (*Anabaena*) in a shallow reservoir. Limnol. Oceanogr. 53 (4), 1227–1241.
Hodges, B.R., Imberger, J., Saggio, A., Winters, K.B., 2000. Modeling basin-scale internal waves in a stratified lake. Limnol. Oceanogr. 45 (7), 1603–1620.
Hozumi, A., Ostrovsky, I., Sukenik, A., Gildor, H., 2020. Turbulence regulation of *Microcystis* surface scum formation and dispersion during a cyanobacteria bloom event. Inland. Waters. 10 (1), 51–70.
Humphries, S.E., Imberger, J., 1982. The Influence of the Internal Structure and the Dynamics of Burrinjuck Reservoir on Phytoplankton Blooms. Environmental Dynamic Report ED 82-023. Centre for Water Research, University Western Australia, Perth, Australia.
Huot, Y., Babin, M., 2010. Overview of fluorescence protocols: theory, basic concepts, and practice. Chlorophyll *a* Fluorescence in Aquatic Sciences: Methods and Applications. Springer, pp. 31–74.
Idso, S.B., 1973. On the concept of lake stability. Limnol. Oceanogr. 18 (4), 681–683.
Karapetyan, N., 2007. Non-photochemical quenching of fluorescence in cyanobacteria. Biochemistry (Moscow) 72 (10), 1127–1135.
Litchman, E., de Tezanos Pinto, P., Klausmeier, C.A., Thomas, M.K., Yoshiyama, K., 2010. Linking traits to species diversity and community structure in phytoplankton. Hydrobiologia 653, 15–28.
Lucius, M.A., Johnston, K.E., Eichler, L.W., Farrell, J.L., Moriarty, V.W., Relyea, R.A., 2020. Using machine learning to correct for nonphotochemical quenching in high-frequency, in vivo fluorometer data. Limnol. Oceanogr.: Methods. 18 (9), 477–494.

MacIntyre, S., 1993. Vertical mixing in a shallow, eutrophic lake: possible consequences for the light climate of phytoplankton. Limnol. Oceanogr. 38 (4), 798–817.
Moore, C.M., Suggett, D.J., Hickman, A.E., Kim, Y.-N., Tweddle, J.F., Sharples, J., Geider, R.J., Holligan, P.M., 2006. Phytoplankton photoacclimation and photoadaptation in response to environmental gradients in a shelf sea. Limnol. Oceanogr. 51 (2), 936–949.
Morrison, J.R., 2003. In situ determination of the quantum yield of phytoplankton chlorophyll *a* fluorescence: a simple algorithm, observations, and a model. Limnol. Oceanogr. 48 (2), 618–631.
Müller, P., Li, X.-P., Niyogi, K.K., 2001. Non-photochemical quenching. A response to excess light energy. Plant Physiol. 125 (4), 1558–1566.
Murchie, E.H., Lawson, T., 2013. Chlorophyll fluorescence analysis: a guide to good practice and understanding some new applications. J. Exp. Bot. 64 (13), 3983–3998.
Pace, M.L., Batt, R.D., Buelo, C.D., Carpenter, S.R., Cole, J.J., Kurtzweil, J.T., Wilkinson, G.M., 2017. Reversal of a cyanobacterial bloom in response to early warnings. Proc. Natl. Acad. Sci. 114 (2), 352–357.
Pace, M.L., Buelo, C.D., Carpenter, S.R., 2021. Phytoplankton biomass, dissolved organic matter, and temperature drive respiration in whole lake nutrient additions. Limnol. Oceanogr. 66 (6), 2174–2186.
Prokopkin, I., Gubanov, V., Gladyshev, M., 2006. Modelling the effect of planktivorous fish removal in a reservoir on the biomass of cyanobacteria. Ecol. Modell. 190 (3–4), 419–431.
Ralston, D.K., Moore, S.K., 2020. Modeling harmful algal blooms in a changing climate. Harmful Algae 91, 101729.
Ranjbar, M.H., Hamilton, D.P., Etemad-Shahidi, A., Helfer, F., 2021. Individual-based modelling of cyanobacteria blooms: physical and physiological processes. Sci. Total Environ. 792, 148418.
Ranjbar, M.H., Hamilton, D.P., Etemad-Shahidi, A., Helfer, F., 2022. Impacts of atmospheric stilling and climate warming on cyanobacterial blooms: an individual-based modelling approach. Water Res. 221, 118814.
Read, J.S., Hamilton, D.P., Jones, I.D., Muraoka, K., Winslow, L.A., Kroiss, R., Wu, C.H., Gaiser, E., 2011. Derivation of lake mixing and stratification indices from high-resolution lake buoy data. Environ. Model. Softw. 26 (11), 1325–1336.
Reynolds, C.S., 1989. Physical Determinants of Phytoplankton Succession. Plankton Ecology, Springer, pp. 9–56.
Roesler, C.S., Barnard, A.H., 2013. Optical proxy for phytoplankton biomass in the absence of photophysiology: rethinking the absorption line height. Methods in Oceanogr. 7, 79–94.
Rousso, B.Z., Bertone, E., Stewart, R.A., Hughes, S.P., Hobson, P., Hamilton, D.P., 2022. Cyanobacteria species dominance and diversity in three Australian drinking water reservoirs. Hydrobiologia 849, 1453–1469.
Rousso, B.Z., Bertone, E., Stewart, R.A., Rinke, K., Hamilton, D.P., 2021. Light-induced fluorescence quenching leads to errors in sensor measurements of phytoplankton chlorophyll and phycocyanin. Water Res. 198, 117133.
Rueda, F.J., MacIntyre, S., 2010. Modelling the fate and transport of negatively buoyant storm–river water in small multi-basin lakes. Environ. Model. Softw. 25 (1), 146–157.
Scheffer, M., Baveco, J., DeAngelis, D., Rose, K.A., van Nes, E., 1995. Super-individuals a simple solution for modelling large populations on an individual basis. Ecol. Modell. 80 (2–3), 161–170.
Shatwell, T., Thiery, W., Kirillin, G., 2019. Future projections of temperature and mixing regime of European temperate lakes. Hydrol. Earth. Syst. Sci. 23 (3), 1533–1551.
Sokolova, E., Pettersson, T.J.R., Bergstedt, O., Hermansson, M., 2013. Hydrodynamic modelling of the microbial water quality in a drinking water source as input for risk reduction management. J. Hydrol. 497, 15–23.
Stow, C.A., Stumpf, R.P., Rowe, M.D., Johnson, L.T., Carrick, H.J., Yerubandi, R., 2022. Model assumptions limit implications for nitrogen and phosphorus management. J. Great Lakes Res. 48 (6), 1735–1737.
Visser, A.W., 1997. Using random walk models to simulate the vertical distribution of particles in a turbulent water column. Mar. Ecol. Prog. Ser. 158, 275–281.
Visser, P.M., Ibelings, B.W., Bormans, M., Huisman, J., 2016. Artificial mixing to control cyanobacterial blooms: a review. Aquatic Ecol. 50 (3), 423–441.
Wallace, B.B., Bailey, M.C., Hamilton, D.P., 2000. Simulation of vertical position of buoyancy regulating *Microcystis aeruginosa* in a shallow eutrophic lake. Aquat Sci 62 (4), 320–333.
Wilkinson, G.M., Carpenter, S.R., Cole, J.J., Pace, M.L., Batt, R.D., Buelo, C.D., Kurtzweil, J.T., 2018. Early warning signals precede cyanobacterial blooms in multiple whole-lake experiments. Ecol. Monogr. 88 (2), 188–203.
Woolway, R.I., Merchant, C.J., 2019. Worldwide alteration of lake mixing regimes in response to climate change. Nat. Geosci. 12 (4), 271–276.
Xiao, M., Burford, M.A., Wood, S.A., Aubriot, L., Ibelings, B.W., Prentice, M.J., Galvanese, E.F., Harris, T.D., Hamilton, D.P., 2022. Schindler's legacy: from eutrophic lakes to the phosphorus utilization strategies of cyanobacteria. FEMS Microbiol. Rev. 46 (6) fuac029.
Xue, P., Pal, J.S., Ye, X., Lenters, J.D., Huang, C., Chu, P.Y., 2017. Improving the simulation of large lakes in regional climate modeling: Two-way lake–atmosphere coupling with a 3D hydrodynamic model of the Great Lakes. J. Clim. 30 (5), 1605–1627.
Zhang, F., Zhang, H., Bertone, E., Stewart, R., Lemckert, C., Cinque, K., 2020. Numerical study of the thermal structure of a stratified temperate monomictic drinking water reservoir. J. Hydrol. Reg. Stud. 30, 100699.
Zhao, Q., Xu, J., Wang, J., Liu, L., 2021. Temporal-spatial features and key factors' analysis of vertical eddy diffusivities in Taihu Lake. China. Environ Sci Pollut Res.. 28, 45506–45518.